Inhibition of Biocorrosion of Aluminum 2024 Aeronautical Alloy by Conductive Ladder Polymer Poly(o-phenylenediamine)

ARTICLE *in* INDUSTRIAL & ENGINEERING CHEMISTRY RESEARCH · JANUARY 2011

Impact Factor: 2.59 · DOI: 10.1021/ie101678x

2 AUTHORS:

Aruliah Rajasekar
TVU
27 PUBLICATIONS **354** CITATIONS
SEE PROFILE

Yen-Peng Ting
National University of Singapore
132 PUBLICATIONS **4,304** CITATIONS
SEE PROFILE

I&EC research
Industrial & Engineering Chemistry Research

ARTICLE

pubs.acs.org/IECR

Inhibition of Biocorrosion of Aluminum 2024 Aeronautical Alloy by Conductive Ladder Polymer Poly(*o*-phenylenediamine)

Aruliah Rajasekar and Yen-Peng Ting*

Department of Chemical and Biomolecular Engineering, National University of Singapore, 4 Engineering Drive 4, Singapore 117576

Supporting Information

ABSTRACT: The present study examines the role of conductive polymer poly(*o*-phenylenediamine) in corrosion inhibition and its antibacterial activity against bacterial biofilm (*Bacillus cereus* ACE4) on aluminum 2024 aeronautical alloy (AA 2024). Poly(*o*-phenylenediamine) (PoPD) was successfully electropolymerized by cyclic voltammetery on AA 2024 using sulfuric acid solution containing *o*-phenylenediamine monomer. The PoPD coating was characterized by Fourier transform infrared (FTIR) spectroscopy and scanning electron microscopy−energy-dispersive X-ray (SEM−EDAX) spectroscopy analysis. The PoPD was polymerized on the metal surface as thin, transparent layers with a ladder conductive polymer structure. Results showed that the charge transfer resistance of the PoPD coating were higher (8.17 KΩ and 3.28 KΩ) when compared to a pristine and bacterial inoculated system (2.60 Ω and 0.23 KΩ). The PoPD coating effectively inhibits the adhesion of biofilm on AA 2024 due to its biocidal property, demonstrating that PoPD is a novel and superior candidate for the inhibition of biocorrosion by *B. cereus* ACE4 in an aeronautical fuel storage tank.

1. INTRODUCTION

Aluminum alloy AA 2024 is used extensively in the aeronautics and aerospace industry, as it offers excellent physical and mechanical properties. However, the alloy is very susceptible to corrosion in chloride-containing media. Pitting corrosion is known to be a major damage mechanism which affects the integrity of the alloy in aerospace applications. The aircraft aluminum alloys contain numerous constituent metals which play an important role in pit formation.[1] Microorganisms foul fuel tanks as airborne contaminants, through water that enters the tank or through contaminated fuel. Accumulation of water in fuel tank permits growth of the microorganisms and may lead to microbiologically induced corrosion (MIC) of the tank structures.[2−5] The occurrence of MIC in the AA 2024 fuel tank may be substantially reduced by coating the fuel tank interiors and through the addition of biostatic additives in jet fuels.[6] Indeed, new applications of conductive polymers in metal coatings to protect the metal against corrosion have been shown to be both effective and environmentally friendly. Owing to their remarkable physical attributes, conductive polymers have been the focus of active research in many technological areas such as rechargeable batteries, sensors, electrochromic display devices, smart windows, molecular devices, energy-storage systems, and membrane gas separation over the past two decades.[7−12] Kendig and Kinlen[13] have well documented the "smart" corrosion inhibiting coatings by conducting polymer doped PANI (polyaniline) on AA 2024 in neutral solutions. Coupling a carbon paste containing polyDMcT to a freshly polished metallic Al surface releases a corrosion inhibiting reduction product from the paste that diffuses to and inhibits a remote cathode.[14−16] Electropolymerization of poly(*o*-phenylenediamine) (PoPD) on stainless steel, platinum, indium tin oxide, and glassy carbon electrodes in sulfuric acid solutions containing *o*-phenylenediamine monomer is an active area of research.[9,17] PoPD was first electrodeposited against corrosion of stainless steel (SS 304) using aqueous solutions of phosphoric acid and sulfuric acid by D'Elia et al.[18] and by Hermas.[11] A literature survey shows that the application of PoPD for biocorrosion inhibition of AA 2024 has not been reported. In this investigation, we report the antimicrobial and anticorrosion properties of surface-functionalized PoPD on *Bacillus cereus* ACE4 biofilm on AA 2024 coupons. The antibacterial activity and anticorrosion efficiency of PoPD were evaluated using electrochemical analysis, total viable cell assays (TVC), fluorescence microscopy (FM), and scanning electron microscopy−energy-dispersive X-ray spectroscopy analysis (SEM−EDAX), in 1% sodium chloride solution.

2. EXPERIMENTAL MATERIALS AND METHODS

2.1. Microorganisms. Hydrocarbon degrading bacterium *Bacillus cereus* ACE4 was isolated from a corrosion product at a diesel-transporting pipeline in the northwestern region of India and was identified as described earlier.[19] The culture was identified by 16S rDNA gene analysis, and the nucleotide sequence data of *B. cereus* ACE4 was deposited in GenBank under accession number AY912105. The ability of the bacteria to grow on hexadecane was determined by inoculating bacterial isolates into test tubes containing a sterile minimal salt medium (MSM) which consists of (grams per liter) $(NH_4)_2SO_4$, 0.22 g; KH_2PO_4, 1.20 g; $MgSO_4 \cdot 7H_2O$, 0.23 g; $CaCl_2$, 0.25 g; yeast extract, 0.024 g with 1% hexadecane. Cultures were shaken at 100 rpm at room temperature (25 °C), and growth was determined by visual inspection (i.e., noting obvious changes in turbidity).

2.2. Chemicals and Preparation of PoPD Electrodes. *o*-Phenylenediamine (PD) and all other chemicals used in this

Received: August 7, 2010
Accepted: December 19, 2010
Revised: December 7, 2010
Published: January 19, 2011

study were purchased from Aldrich Chem. Co. The chemicals were commercially available as analytical grade and were used without further purification. All solutions were prepared using deionized water. Electropolymerization and subsequent electrochemical studies were carried out in a conventional three electrode cell, with AA 2024 as the working electrode, Ag/AgCl, in saturated KCl as the reference electrode, and platinum as the counter electrode. AA 2024 of nominal composition (wt %) 0.06% Si, 0.14% Fe, 4.5% Cu, 0.9% Mn, 1.8% Mg, 0.1% Cr, 0.25% Zn, 0.15% Ti, and the remaining Al, was purchased from Metal Samples Company, Alabama Laser Technologies, USA. The coupons (10 mm diameter × 2 mm thickness) were sequentially ground with a series of grit silicon carbide papers (grades 180, 500, 800, 1200, and 1500) to a smooth surface and were finally polished to a mirror finish surface using 0.3 μm alumina powder. The polished coupons were rinsed with deionized water and then dipped in 5% NaOH solution for 2 min to activate the surface.[12] After this stage, the samples were cleaned with cleaning powder to remove the black colored smudge formed over the surface and were washed thoroughly with running water and dipped in conc. HNO_3 solution for 30 s. The activated coupons were used for the PoPD coating and surface analysis (i.e., SEM and Fourier transform infrared spectroscopy (FTIR)). Poly(*o*-phenylenediamine) was deposited on AA 2024 alloy by cyclic voltammetery (CV) in the potential window −0.5 and 1.2 V (Ag/AgCl) from 0.1 M sulfuric acid solution of pH 1.0 containing 0.05 M *o*-phenylenediamine at room temperature (25 °C). The poly(*o*-phenylenediamine) structure was confirmed by the FTIR spectrophotometer using a Bio-Rad Model: FTS 135 and a scanning electron microscope (SEM-JEOL, model JSM-5600). Electrochemical measurements were made using an Autolab PGSTAT12 potentiostat/galvanostat/ZRA system (USA). Atomic force microscopy (AFM) analyses were carried out to visualize the PoPD film formed on the metal surface and estimate the surface roughness. The pristine and coated PoPD coupons were examined using a Nanoscope IIIA AFM (Digital Instruments, USA) in the tapping mode to capture the images of PoPD film on the AA 2024 surface. Silicon nitride (Si_3N_4) cantilever nanoprobes, with a spring constant of k = 0.06 N/m (Digital Instruments, USA), were used. Low contact force was chosen to reduce deformation of the PoPD film surfaces.

2.3. Biocorrosion Studies. Biocorrosion studies were performed (using duplicate coupons) at 25 °C for 10 days in 1% NaCl electrolyte. System I consisted of 500 mL of sterile MSM broth and pristine (i.e., noncoated) coupons as the control. System II consisted of System I inoculated with 2 mL of *B. cereus* ACE4 at about 10^6 CFU/mL. System III consisted of System I but with PoPD coated coupons. System IV consisted of System II but with coated PoPD coupons and was inoculated with *B. cereus* ACE4 (10^6 CFU/mL). All the experiments were conducted in a corrosive environment with 1% sodium chloride as the electrolyte. Hexadecane (1%) was added in all the systems to simulate a fuel/water environment. Biocorrosion experiments were initiated by hanging pristine and PoPD coated coupons on a nylon string in both the medium with and without the bacteria. After 10 days, the coupons were removed for electrochemical, FTIR, and SEM−EDAX analysis. Electrochemical impedance spectroscopy (EIS) measurements (using duplicate coupons) were performed ex situ; the coupons that were removed from the appropriate systems served as the working electrodes, each with an exposed surface area of 0.785 cm^2 (Metrohm Pte. Ltd.). The electrolyte comprised 200 mL of the medium from each system.

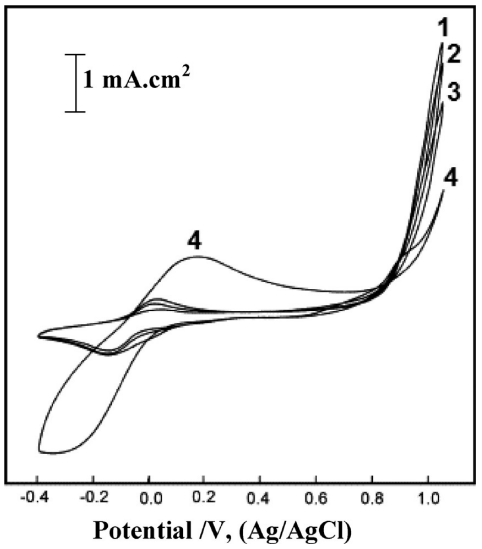

Figure 1. Cyclic voltamogram for electrodeposition PoPD on AA 2024 in 0.1 M H_2SO_4 containing 0.05 M *o*-phenylenediamine.

EIS measurements were made after steady-state open circuit potential (OCP) using a 10 mV amplitude sinusoidal signal over frequencies ranging from 5 mHz to 100 kHz. Tafel plots were recorded by scanning from the open circuit potential (E_{corr}) toward the 200 mV anodically and −200 mV cathodically using duplicate coupons at a scan rate of 0.5 mV s^{-1}. Impedance and potentiodynamic polarization studies were conducted using the same coupons, with care taken to minimize any disturbance to the oxide film. The corrosion protection efficiency (CPE) of the coating (both in the absence and presence of the bacteria) was calculated by comparing the change (i.e., a decrease) in the corrosion current density (derived from Tafel polarization curves)

2.4. Evaluation of Antibacterial Activity of PoPD. Antibacterial activity of the PoPD coating on AA 2024 was evaluated using total viable count (TVC) assay, SEM, and fluorescence microscopy. To enumerate the TVC, PoPD-coated coupons with *B. cereus* ACE4 biofilm were removed from Systems II and IV. Using a sterile brush, the biofilm on the coupons in these systems were dispersed into 10 mL of sterile phosphate buffer (0.0425 g of KH_2PO4 and 0.19 g of $MgCl_2$ per liter) and vortexed to disperse the bacterial cells. Serial dilutions of the bacterial cell suspension were prepared, and 0.1 mL of each dilution was spread plated onto MSM agar. The plates were incubated at 25 ± 2 °C for 24−48 h, and the TVC was enumerated. The sample fixation and preparation for SEM imaging has been described earlier.[20] The ability of the coated PoPD coating in inhibiting bacterial adhesion of *B. cereus* ACE4 was revealed through SEM images. To observe surface corrosion, the bacterial cells and the corrosion products were removed from the coupon surface as described earlier.[4] The bactericidal characteristics of the coupons were evaluated using optical fluorescence microscopy (FM- Olympus America Inc., NY).

3. RESULTS AND DISCUSSION

3.1. Electrodeposition of PoPD Films on Aluminum Alloy 2024. As the bare AA 2024 electrode was immersed in 0.1 M H_2SO_4 (pH 1) solution containing 0.05 M *o*-phenylenediamine, its OCP shifted to the positive side and a passive film was formed within a few minutes. Figure 1 shows the cyclic voltammogram

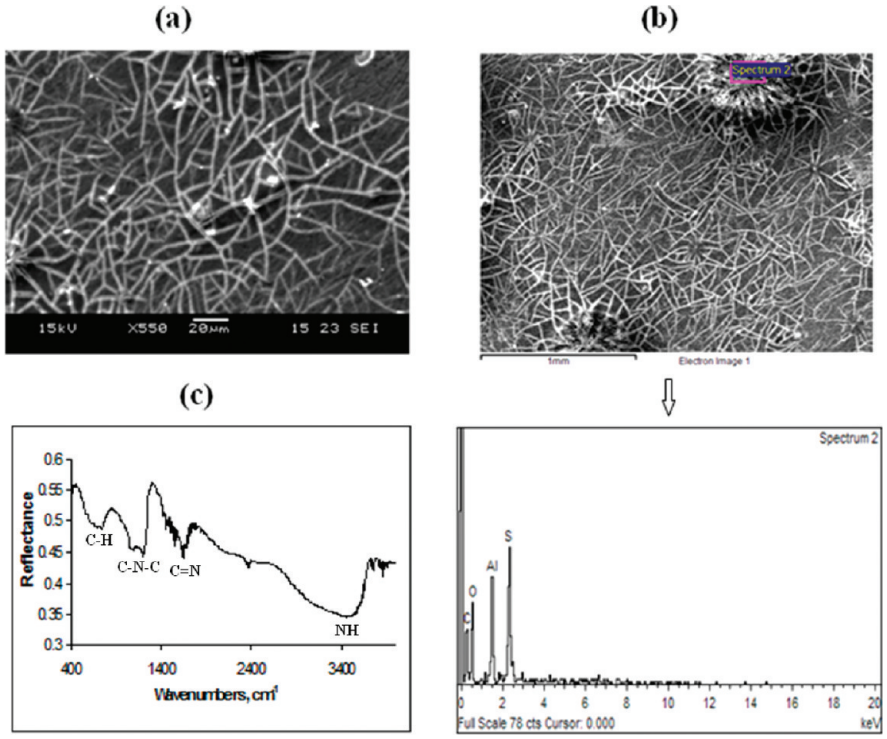

Figure 2. Characterization of PoPD layers on AA 2024 surface. (a) SEM morphology of PoPD coated surface, (b) SEM−EDAX analysis of the PoPD coated surface, and (c) FTIR spectrum of PoPD coated surface.

for the redox behavior of PoPD on the AA 2024 in 0.1 M H_2SO_4. The voltammogram shows irreversible peaks at potentials higher than 1.0 V (Ag/AgCl), which resulted from the formation of red color film on the electrode surface. This corroborates an earlier report on PoPD on stainless steel (Hermas et al., 2006). On the first reverse scan, the cathodic current peak appeared at about −0.2 V and the anodic peak appeared on the second forward scan at about −0.02 V, with slight variation in the subsequent cycles. No further current increase was recorded after about 20 cycles, and a thin, adherent layer was formed on the electrode surface after these cycles. The polymer layer appeared reddish-brown in the oxidized state and had a greenish coloration in the reduced state. These results corroborate the observation by Hermas[11] and D'Elia et al.[18]

3.2. Morphology Study of PoPD Films. The morphology, thickness, and chemical composition of PoPD layers on the metal were investigated using SEM−EDAX and FTIR (Figure 2a−c). As aforementioned, a transparent and compact polymer layer (more than 1.0 μm) of PoPD formed after 20 cycles, as shown in Figure 2a. The layer of PoPD is characterized by a network of broad threadlike fibers (0.3−0.8 μm) which appeared shiny silver and reflective. These fibers were similar to those which appeared in transparent films of ladder conductive polymer PoPD on stainless steel (Hermas 2008). EDAX analysis showed that the sulfur content in the PoPD coated metal was about 6.23 wt % (Figure 2b). The PoPD films prepared on AA 2024 were measured using an FTIR spectrometer (Figure 2c). The spectrum of PoPD film on the coupon shows absorption at wave numbers at 3300−3400 cm^{-1}, indicating the presence of −N−H stretching band, and at about 1546 cm^{-1}, indicating C═N vibration from the phenazine ring.[11] The absorption peaks at 1390 and 1240 cm^{-1} were ascribed to the stretching of C−N bond in the aromatic ring present in the PoPD film. The broad band at 1120 cm^{-1} can be ascribed to the C−N−C stretching bond, which overlaps the peak of sulfate ions which were incorporated during the electrodepostion of PoPD. The band at 760−960 cm^{-1} indicates the presence of C−H out-of-plane bending mode, and the absorption peaks at 762, 847, 900, and 947 cm^{-1} indicate the substituted benzene structure present in the PoPD film. The FTIR and SEM−EDAX analyses show that the PoPD coating was strongly adsorbed on the surface of AA 2024 with the coordination with sulfate SO_4^{2-} ion and lone pair electrons of the aromatic diamine during electropolymerization with H_2SO_4. AFM images of the pristine and PoPD coated coupons are shown in Figure S1A,B, Supporting Information. The surface roughness of the pristine and coated coupons was 45.2 and 709 nm, respectively. The higher surface roughness of the coated alloy was due to the formation of a thin, adherent PoPD film on the metal surface.

3.3. Corrosion Protection Performance and Antibacterial Activity of PoPD Coating. Figure 3 shows the potentiodynamic polarization curves for AA 2024 in 1% NaCl solution in the presence and in the absence of *B. cereus* ACE4 and PoPD coated coupons. The corresponding data are presented in Table 1. The corrosion potential for the control (i.e., System I) was −525 mV vs Ag/AgCl. In the presence of the *B. cereus* ACE4, the potential of the AA 2024, at −437 mV on the 10th day, shifted toward the anodic direction. However, in the PoPD coated system, with and without the bacteria, the potential (at −456 and −362 mV, respectively) increases toward the noble direction. These results indicate that PoPD forms an intact passive layer on the AA 2024 surface. The PoPD coated system reduced the corrosion current (2.8×10^{-4} A/cm^2) by several orders of magnitude compared to the bacterial System II (at 1.48 A/cm^2) and the control System I (at 1.5×10^{-3} A/cm^2). The corrosion rates of PoPD coated metal in the absence or presence of bacterium were highly reduced when compared to control system I and bacterial system II. The

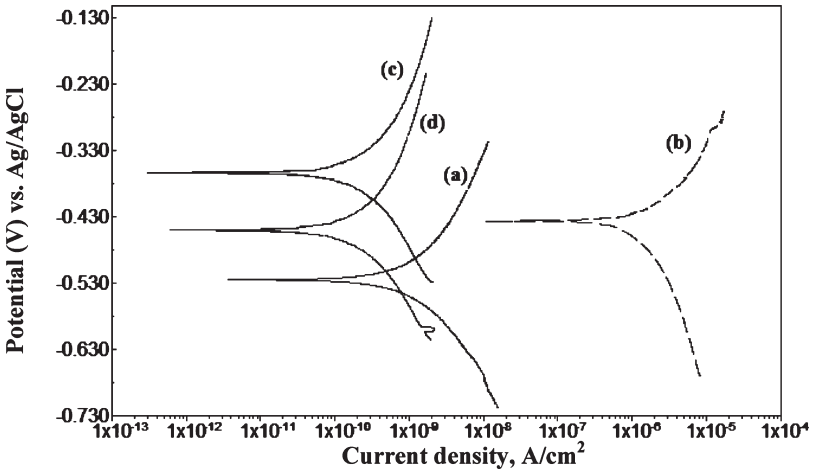

Figure 3. Tafel plots for (a) pristine AA 2024, System I; (b) pristine AA 2024 inoculated with *B. cereus* ACE4, System II; (c) PoPD coated AA 2024, System III; (d) PoPD coated AA 2024 inoculated with *B. cereus* ACE4, System IV.

Table 1. Tafel and Impedance Parameters for Pristine and PoPD Coated AA 2024 in the Presence and Absence of *B. cereus* ACE4 Exposed to a 1% NaCl Solution

	polarization data				impedance data	
system no.	corrosion potential, E_{corr} (mV)	corrosion current, i_{corr} (A/cm^2)	corrosion rate (mm/y)	protection efficiency (%)	solution resistance, R_s (KΩ)	charge transfer resistance, R_{ct} (KΩ)
I	−525	1.5×10^{-3}	1.5×10^{-5}		0.14	2.60
II	−437	1.48	3.49×10^{-2}		0.21	0.23
III	−362	2.8×10^{-4}	3.29×10^{-6}	81	0.12	8.17
IV	−456	2.5×10^{-4}	2.9×10^{-6}	99.9	0.10	3.28

corrosion protection efficiencies of the PoPD coating on AA 2024, in the absence (i.e., comparing System III and System I) or presence of the bacterium (i.e., comparing Systems IV and System II), was found to be 81% and almost 100%, respectively. Compared with the control, the presence of *B. cereus* ACE4 significantly accelerated the corrosion rate of the pristine coupons by 3 orders of magnitude (i.e., from 1.5×10^{-5} to 3.49×10^{-2} mm/y). The polarization curve for AA 2024 in the presence of *B. cereus* ACE4 shows enhancement of both anodic and cathodic reactions when compared to other systems. In the PoPD System III and IV, the nature of both the anodic and cathodic curves is shifted to the cathodic direction, thus indicating that PoPD suppresses both the anodic and cathodic reaction significantly. The corrosion resistances of PoPD coated films, evaluated as electrochemical impedance, at OCP in 1% sodium chloride are presented in Figure 4a,b. The solution resistance (R_s) and the charge transfer resistance (R_{ct}) were derived from impedance measurements and are presented in Table 1. The R_s values for all the systems fall in the range of 0.10−0.21 KΩ. The R_{ct} values in Systems I and II, at 2.60 and 0.23 KΩ, respectively, increased to 8.17 and 3.28 kΩ in the PoPD coated coupons. The increase in R_{ct} could be attributed to the strong adsorption of the diamine species on the metal, thus increasing the corrosion resistance.[21] This observation is consistent with our polarization studies where high frequency semicircles (when compared to Systems I and II (Figure 4b)) were noted in Systems III and IV. The high capacitive loop is well-defined with a high-frequency range. The high-frequency part represents the formation of the intact part of the adsorbed film. The hetero atoms (nitrogen and oxygen) present in the PoPD film coordinate with aluminum oxide to form a thick oxide layer on the AA 2024 surface to suppress both cathodic and anodic reactions. In Systems I and II, the capacitive loop is relatively small when compared to Systems III and IV, due to the defects and pores in the adsorbed film on the metal surface. The PoPD coating on the metal (i.e., Systems III and IV) results in an increase in the corrosion protection efficiency (CPE) of 83% and 99.9% respectively, as calculated from the potentiodynamic polarization data. These results manifest the effectiveness of PoPD polymer in protecting the AA 2024 coupons against biocorrosion.

The viable count assay in the PoPD coated biofilm was reduced to about 1.54×10^2 CFU/cm^2 of the coupon surface when compared to the pristine coupon (2.69×10^8 CFU/cm^2 of coupon surface) after the biocorrosion experiment. Figure 5 shows the SEM images of the corresponding pristine and PoPD coated AA 2024 alloy (i.e., Systems II and IV). The surface of the pristine coupon with *B. cereus* ACE4 revealed a thick biofilm along with large quantities of corrosion products, whereas the PoPD coated coupon showed less biofilm. Fluorescence images showed dense biofilm of *B. cereus* ACE4 attached on the pristine metal surface and much less dense biofilm on the surface-modified metal (Figure 5b,d). AFM results revealed an increase in surface roughness of the PoPD coated surface due to the thin film formation (Figure S1B, Supporting Information), a phenomenon which should enhance greater bacterial adhesion. However, results showed that the coated PoPD polymer successfully reduced bacterial adhesion and the production of biofilm on the coupon due to their antibacterial activity. SEM−EDAX analysis was

dx.doi.org/10.1021/ie101678x |*Ind. Eng. Chem. Res.* 2011, 50, 2040–2046

carried out to examine the surface morphology and elemental composition of the AA 2024 coupons (Figure 6a−d). In systems with pristine coupons, more corrosion pits were evident in the presence of the bacteria (compare Figure 6b,a). Figure 6c,d also shows that PoPD coating conferred protection against pitting corrosion. EDAX analysis show that these corrosion deposits in the presence of *B. cereus* ACE4 contain a high 98 wt % of aluminum, magnesium, and carbon when compared to the control (70 wt %), PoPD coated System III (30 wt %) and System IV (40 wt %). These results, which show fewer corrosion pits in systems with PoPD coated coupons, are consistent with Figure 6 and, hence, confirm the antibacterial properties of the surface modified AA 2024.

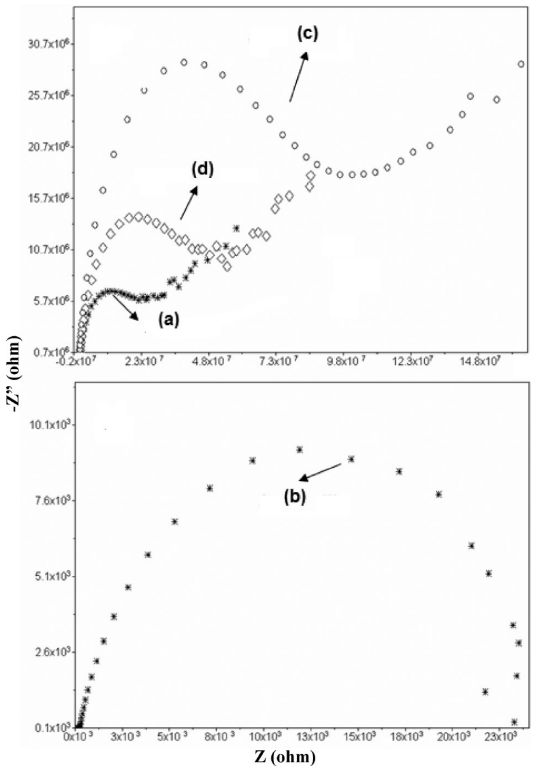

Figure 4. Nyquist plots for (a) pristine AA 2024, System I; (b) pristine AA 2024 inoculated with *B. cereus* ACE4, System II; (c) PoPD coated AA 2024, System III; (d) PoPD coated AA 2024 inoculated with *B. cereus* ACE4, System IV.

3.4. Mechanism of Biocorrosion Inhibition. Pitting is a highly localized type of corrosion in the presence of aggressive chloride ions. Pits are initiated by chloride attack at weak sites in the metal oxide.[22,23] The pits propagate according to reactions 1 and 2

$$Al \leftrightarrow Al^{3+} + 3e^- \quad (1)$$

$$Al^{3+} + 3H_2O \leftrightarrow Al(OH)_3 + 3H^+ \quad (2)$$

while hydrogen evolution and oxygen reduction are the important reduction processes at the intermetallic cathodes.

$$2H^+ + 2e^- \rightarrow H_2 \quad (3)$$

$$O_2 + 2H_2O + 4e^- \rightarrow 4OH^- \quad (4)$$

As a pit propagates, the environment within the pit (i.e., the anode) changes and the pH decreases (see reaction 2). The positive charges also cause the migration of chloride ions into the pit, resulting in HCl formation which further accelerates the pit propagation (Figure 6a). The reduction reaction causes local alkalinization around the cathodic particles. Aluminum oxide is not stable in such an environment, and aluminum around the particles will dissolve the pits. The active aluminum component of the particles will also dissolve selectively, thereby enriching the

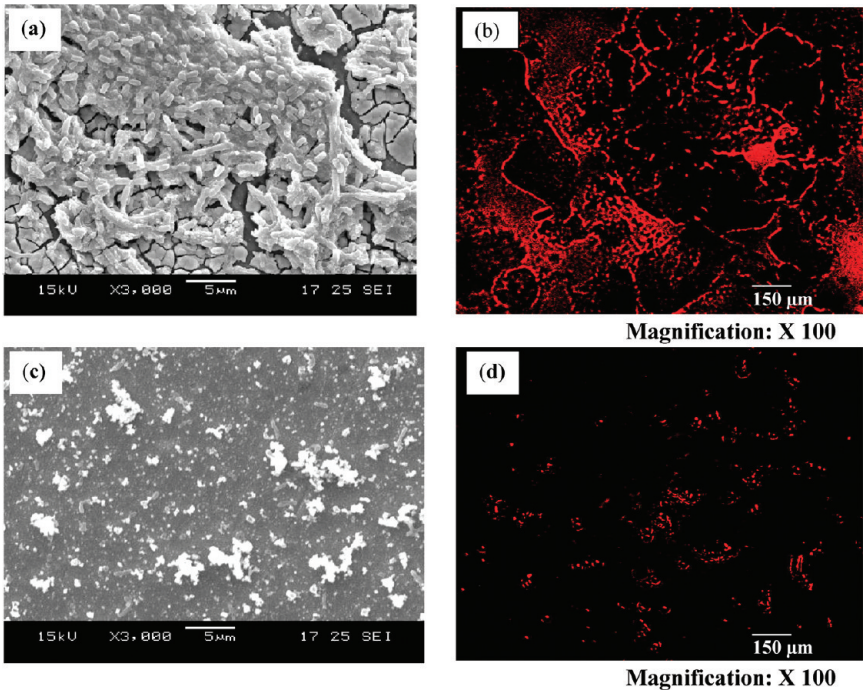

Figure 5. SEM and fluorescence images of *B. cereus* ACE4 biofilm in 1% NaCl solution after 10 days; (a,b) pristine AA 2024 and (c,d) PoPD coated AA 2024.

dx.doi.org/10.1021/ie101678x |*Ind. Eng. Chem. Res.* 2011, 50, 2040–2046

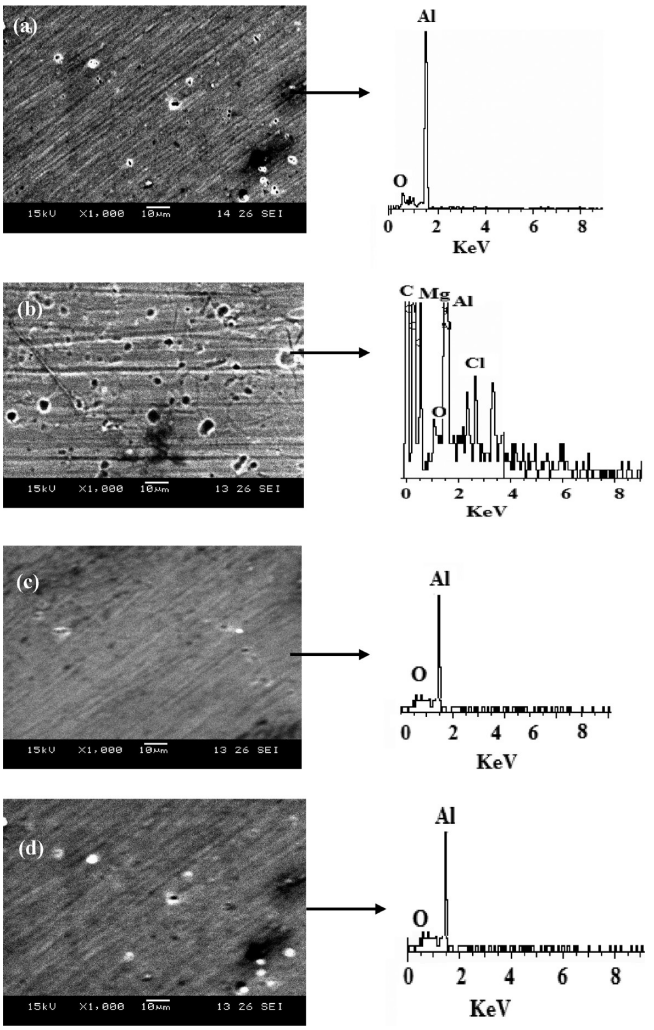

Figure 6. SEM images and their corresponding EDS analysis of pristine and PoPD coated AA 2024 immersed in 1% NaCl solution for 10 days (a) pristine AA 2024, System I; (b) pristine AA 2024 inoculated with *B. cereus* ACE4, System II; (c) PoPD coated AA 2024, System III; (d) PoPD coated AA 2024 inoculated with *B. cereus* ACE4, System IV.

particle surface with aluminum oxide and increasing its cathodic activity. Etching of the aluminum matrix around the particles may detach the particles from the surface, which may repassivate the alkaline pits.[24] This may also reduce the driving force for the acidic pits, thus causing repassivation of some in the long run. The PoPD plays a significant role in the protection and in the formation of passive oxides on the Al alloy. Due to the low permeability of PoPD films, oxygen diffusion is hindered, which in turn reduces the rate of the oxygen reduction reaction given below. Anodically produced aluminum ions form metal coordinate ligand with hetero atoms (nitrogen and oxygen) present in the PoPD. Subsequently, the cathodic reaction is suppressed due to the lack of electrons. The PoPD conductive polymer can also be reoxidized by atmospheric or dissolved oxygen as per the reaction given below.[24] CP represents the conductive polymer.

$$n/4\,O_2 + n/2\,2H_2O + CP^{o} \rightarrow CP^{n+} + OH^{-} \qquad (5)$$

SEM microphotograph of PoPD films shows a compact continuous fiberlike structure (Figure 2a) which inhibits the diffusion of oxygen molecules. The impedance data (Table 1) show that R_{ct} increased in the presence of PoPD coating, in comparison with the pristine metal. PoPD may be represented as ladder polymer containing phenazine rings[17] with an asymmetrical "quinoid" structure. The expected redox reaction in the acid solution is shown in reaction 6.

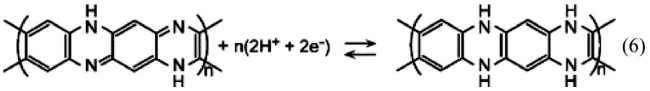

(6)

In petroleum transporting pipeline and storage tank, corrosion can develop as pitting at the fuel−water interface. Oxidation of petroleum hydrocarbon by this bacterium[4,25] produces organic acids and reduces the pH of the medium. The oxidation reaction consumes the oxygen dissolved in naphtha fuel and in water. The bacterial enzymes preferentially attack zinc and magnesium present in AA 2024.[4,26,27] The microbial corrosion is impeded by the inhibition in the growth of bacteria biofilm on the functionlized PoPD AA 2024. Phenylenediamine derivatives have been reported to be inhibitory to microbial oxidation processes in activated sludge and in streamwater.[28] Ogawa et al.[29] demonstrated that azo dyes inhibited the respiration of microorganisms in activated sludge. The inhibitory effect of phenylenediamine was possibly due to the aromatic amines, including benzamines, generated by azo reduction, which is known to occur widely in the environment.[30,31] Inhibition of bacterial adhesion is correlated with the concentration of positively charged nitrogen (N^{+}) species on the coupon surface. As shown in SEM Figure 5a, the number of bacterial cells adhered to the PoPD coated AA 2024 surfaces were significantly reduced. The bacterial cells were sparsely distributed as single cells, with disimilar shapes. The deformation in bacterial shape and the reduction in cell count suggest that the surface-bearing polycationic N^{+} species exert bactericidal effects on *B. cereus* ACE4.[32] It has been reported that the nitro-group present in PoPD causes mutagenicity of the bacterial metabolites.[33−37] Our data clearly indicate that *o*-phenylenediamine was inhibitory to the growth of *B. cereus* ACE4 biofilm on AA 2024 surface.

4. CONCLUSIONS

A novel approach to combat biocorrosion through the use of polymer coating of poly (*o*-phenylenediamine) (PoPD) on AA 2024 surfaces, via electrochemical polymerization, was examined. Electrochemical analysis revealed that the PoPD coating significantly reduced the corrosion current when compared to pristine samples. FTIR and SEM studies show that the PoPD film coat onto the AA surface via their diamine species coordination with aluminum oxide to form a thick passive layer which suppresses both the anodic and cathodic reactions. The nitro-group in *o*-phenylenediamine confers antibacterial properties of PoPD-coated AA 2024 and, thus, inhibits bacterial adhesion and growth on AA 2024. Compared to the pristine alloy in the absence and presence of bacteria, the PoPD coated systems showed corrosion protection efficiencies of about 81% and almost 100%, respectively, on the basis of the corrosion current density. The PoPD polymer is shown to be a good candidate for the protection of AA 2024 against biocorrosion by *B. cereus* ACE4.

■ ASSOCIATED CONTENT

Supporting Information. AFM images of AA 2024 metal surfaces. This material is available free of charge via the Internet at http://pubs.acs.org.

AUTHOR INFORMATION

Corresponding Author
*E-mail: chetyp@nus.edu.sg.

ACKNOWLEDGMENT

The authors would like to thank the National University of Singapore for financial support of this study under an FRC Research Grant R-279-000-227-112.

REFERENCES

(1) Strehblow, H. H. Mechanisms of pitting corrosion. *Corrosion mechanisms in theory and practice*; Marcel Dekker, Inc.: New York, 1995; pp 201−238.

(2) Fang, H. H. P.; Xu, L.-C.; Chan, K.-Y. Effects of toxic metals and chemicals on biofilm and biocorrosion. *Water. Res.* **2002**, *31*, 4709–4716.

(3) Groysman, A. In *Corrosion for Everybody*; Springer: New York, 2010; p 368, ISBN: 978-90-481-3476-2.

(4) Rajasekar, A.; Ting, Y. P. Microbial corrosion of aluminum 2024 aeronautical alloy by hydrocarbon degrading bacteria *Bacillus cereus* ACE4 and *Serratia marcescens* ACE2. *Ind. Eng. Chem. Res.* **2010**, *49*, 6054–6061.

(5) Nercessian, D.; Francisco, B. D.; Desimone, M.; Simison, S.; Busalmen, J. P. Metabolic turnover and catalase activity of biofilms of *Pseudomonas fluorescens* (ATCC 17552) as related to copper corrosion. *Water Res.* **2010**, *44*, 2592–2600.

(6) Mansfeld, F.; Little, B. A technical review of electrochemical techniques applied to microbiologically influenced corrosion. *Corros. Sci.* **1991**, *32*, 247–272.

(7) Sexena, V.; Malhotra, B. D. Prospects of conducting polymers in molecular electronics. *Curr. Appl. Phys.* **2003**, *3*, 293–305.

(8) Wang, Y.; Jing, X. Intrinsically conducting polymers for electromagnetic interference shielding. *Polym. Adv. Technol.* **2005**, *16*, 344–351.

(9) Martinusz, K.; Inzelt, G.; Horanyi, G. Coupled electrochemical and radiometric study on anion migration in poly(o-phenylenediamine) films. *J. Electroanal. Chem.* **1995**, *395*, 293–297.

(10) Karpagam, V.; Sathiyanarayanan, S.; Venkatachari, G. Studies on corrosion protection of Al2024 T6 alloy by electropolymerized polyaniline coating. *Curr. Phys.* **2008**, *8*, 93–98.

(11) Hermas, A. A. Protection of type 430 stainless steel against pitting corrosion by ladder conductive polymer. *Prog. Org. Coat.* **2008**, *61*, 95–102.

(12) Kamaraj, K.; Sathiyanarayanan, S.; Venkatachari, G. Electropolymerised polyaniline films on AA 7075 alloy and its corrosion protection performance. *Prog. Org. Coat.* **2009**, *64*, 67–73.

(13) Kendig, M.; Kinlen, P. Demonstration of Galvanically Stimulated Release of a Corrosion Inhibitor Basis for "Smart" Corrosion Inhibiting Materials. *J. Electrochem. Soc.* **2007**, *154*, C195–C201.

(14) Kendig, M.; Hon, M.; Kinlen, P. 'Smart' corrosion inhibiting coatings. *Prog. Org. Coat.* **2003**, *47*, 183–189.

(15) Kendig, M.; Jeanjaquet, S. Cr(VI) and Ce(III) inhibition of oxygen reduction on copper. *J. Electrochem. Soc.* **2002**, *149*, B47–B51.

(16) Skorb, E. V.; Fix, D.; Andreeva, D. V.; Mohwald, H.; Shchukin, D. G. Surface-modified mesoporous SiO_2 containers for corrosion protection. *Adv. Funct. Mater.* **2009**, *19*, 2373–2379.

(17) Hermas, A. A.; Wu, Z. X.; Nakayama, M.; Ogura, K. Passivation of stainless steel by coating with poly(o-phenylenediamine) conductive polymer. *J. Electrochem. Soc.* **2006**, *153*, B199–B205.

(18) D'Elia, L. F.; Ortiz, R. L.; Marquez, O. P.; Marquez, J.; Martinez, Y. Electrochemical deposition of poly(o-pheylendiamine) film on type 304 stainless steel. *J. Electrochem. Soc.* **2001**, *148*, C297–300.

(19) Rajasekar, A.; Anandkumar, B.; Maruthamuthu, S.; Ting, Y. P.; Rahman Pattanathu, K. S. M. Characterization of corrosive bacterial consortia isolated from petroleum-product-transporting pipelines. *Appl. Microbiol. Biotechnol.* **2010**, *85*, 175–1188.

(20) Sheng, X.; Ting, Y. P.; Pehkonen, S. O. The influence of ionic strength, nutrients and pH on bacterial adhesion to metals. *J. Colloid Interface Sci.* **2008**, *321*, 256–264.

(21) Ashassi-Sorkhabi, H.; Amri, N. Polarization and impedance methods in corrosion inhibition study of carbon steel by amines in petroleum−water mixtures. *Electrochim. Acta* **2002**, *47*, 2239–2244.

(22) Jones, D. A. *Principles and Prevention of Corrosion*; Prentice-Hall: Upper Saddle River, NJ, 1996; p 213.

(23) Christie, R. M. *Colour Chemistry*; RSC: Cambridge, UK, 2001; p 287.

(24) Vargel, C. In *Corrosion of aluminium*; Elsevier: Boston, 2004; p 308−311.

(25) Rajasekar, A.; Ganesh Babu, T.; Karutha Pandian, S.; Maruthamuthu, S.; Palaniswamy, N.; Rajendran, A. Biodegradation and corrosion behaviour of *Bacillus cereus* ACE4 in diesel transporting pipeline. *Corros. Sci.* **2007**, *49*, 2694–2710.

(26) Hedrick, H. G.; Crum, M. G.; Reynolds, R. J.; Culver, S. C. Mechanism of microbiological corrosion of aluminum alloys. *Electrochem. Technol.* **1967**, *5*, 75–77.

(27) Hedrick, H. G. *Microbiological corrosion of aluminium*; 25th Conference NACE, Houston, Texas, 1970; p 609−619.

(28) Hunter, J. V. The effect of dyes on aerobic systems. In *Dyes and the Environment*; American Dye Manufacturers Institute: New York, 1973; Vol. 1, Chapter 6.

(29) Ogawa, T.; Yamada, Y.; Idaka, E. The respiratory inhibition of activated sludge by dyes. *Soc. Fiber Sci. Technol. Jpn.* **1978**, *34*, T175–180.

(30) Chung, K. T.; Stevens, S. E., Jr .Degradation of azo dyes by environmental microorganisms and helminthes. *Environ. Toxicol. Chem.* **1993**, *12*, 2121–2132.

(31) Chung, K. T.; Murdock, C. A.; Stevens, S. E., Jr.; Li, Y. S.; Wei, C. I.; Fernando, S. Y.; Chou, M. W. Effects of the nitro-group on the mutagenicity and toxicity of some benzamines. *Environ. Mol. Mutagen.* **1996**, *27*, 67–74.

(32) Tiller, J. C.; Liao, C. J.; Lewis, K.; Klibanov, A. M. Designing surfaces that kill bacteria on contact. *Proc. Natl. Acad. Sci. U.S.A.* **2001**, *11*, 5981–5985.

(33) Chung, K. T.; Murdock, C. A.; Stevens, S. E., Jr.; Li, Y. S.; Wei, C. I.; Huang, T. S.; Chou, M. W. Mutagenicity and toxicity studies of *p*-phenylenediamine and its derivatives. *Toxicol. Lett.* **1995**, *8*, 13–24.

(34) Lin, J.; Qiu, S. Y.; Lewis, K.; Klibanov, A. M. Mechanism of bactericidal and fungicidal activities of textiles covalently modified with alkylated polyethylenimine. *Biotechnol. Bioeng.* **2003**, *83*, 168–172.

(35) Milovic, N. M.; Wang, J.; Lewis, K.; Klibanov, A. M. Immobilized N-alkylated polyethylenimine avidly kills bacteria by rupturing cell membranes with no resistance developed. *Biotechnol. Bioeng.* **2005**, *90*, 715–722.

(36) Yuan, S. J.; Xu, F. J.; Pehkonen, S. O.; Ting, Y. P.; Neoh, K. G.; Kang, E. T. Grafting of antibacterial polymers on stainless steel via surface-initiated atom transfer radical polymerization for inhibiting biocorrosion by *Desulfovibrio desulfuricans*. *Biotechnol. Bioeng.* **2009**, *103*, 268–281.

(37) Yuan, S. J.; Xu, F. J.; Pehkonen, S. O.; Ting, Y. P.; Neoh, K. G.; Kang, E. T. Antibacterial Inorganic-Organic Hybrid Coatings on Stainless Steel via Consecutive Surface-Initiated Atom Transfer Radical Polymerization for Biocorrosion Prevention. *Langmuir* **2010**, *26*, 6728–6736.